LAUNCH CAMPAIGN OF THE DECAN LOWER STAGE AND DEVELOPMENT PROGRESS OF A 3D-PRINTED EXPERIMENTAL ROCKET AT TU BERLIN.

J. Léglise[1], T. Nitschke[1], A. Balke[1], J. Stamm[1], H. Adirim[2]
[1]Technische Universität Berlin, Marchst. 12, 10587 Berlin, Berlin, Germany
[2]Aerospace Institute, Marchst. 12, 10587 Berlin, Berlin, Germany

Abstract

This paper describes the current development status of the DECAN rocket project at the Technische Universität Berlin. The hot water powered first stage of the rocket, the solid propellant powered, and the 3D-printed upper stage are presented. The two-stage sounding rocket project offers the students involved the ability to work on a hands-on project in various engineering fields. In March 2017, the engineering qualification model of the DECAN lower-stage was launched as a single-stage rocket from a Bundeswehr test range, near Berlin, in Germany. The launch campaign will be described in this document. Moreover, the development of a 3D-printed experimental rocket structure, which is part of the DECAN rocket's new features, will be presented. The design of the 3D-printed rocket structure is based on the flight proven DECAN-SHARK rocket.

1. INTRODUCTION

The DECAN program (DEutsche CANsat-Höhenrakete) is a student project within the framework of the STERN (STudentische Experimental-RaketeN) project of the German Aerospace Center (DLR). Engineering students get the opportunity to perform hands-on work on a real aerospace project under professional supervision. The different phases of the project follow the ECSS guidelines and are frequently reviewed together with the DLR.
Herein, we describe the current development status of the rocket at the Technische Universität Berlin, which includes a description of the different subsystems. As of now, the DECAN team has successfully launched both the engineering qualification model (EQM) and the flight model (FM) of the DECAN upper-stage (SHARK I&II - Student High Altitude Rocket in Kiruna). Additionally, the EQM of the lower stage (DECAN AQUARIUS) was successfully launched in spring of 2017. A two-staged rocket will be launched in a follow-up project phase. Furthermore, the development progress of a 3D-printed experimental rocket will be presented.

2. TWO-STAGE ROCKET ARCHITECTURE

The rocket consists of a two-stage rocket with a take-off mass of less than 150 kg. DECAN will be capable of launching a CanSat to an altitude of up to 7 km, once the project is completed. The first stage is comprised of a hot water propulsion system developed at TU Berlin. The water is heated to about 270 °C, which produces a pressure of approximately 55 bar inside the vessel. After the takeoff of the rocket, the lower stage produces an average thrust of 2.2 kN for approximately 5 s. The second stage of the rocket is propelled by a solid rocket motor. This stage delivers the main payload, a CanSat, to the desired altitude. FIG 1 shows a CAD model of the two-staged DECAN rocket mounted on the launch rail. Both stages have been configured in such a way as to allow them to be flown independently from each other. The relatively low apogee height of the first stage (approximately 1 km) allows the team to launch from nearby test ranges. Hence, hardware and software components can be tested frequently. The image shows the interstage adapter used in a two-stage configuration. In single-stage operation, the interstage adapter is replaced by a nose cone.

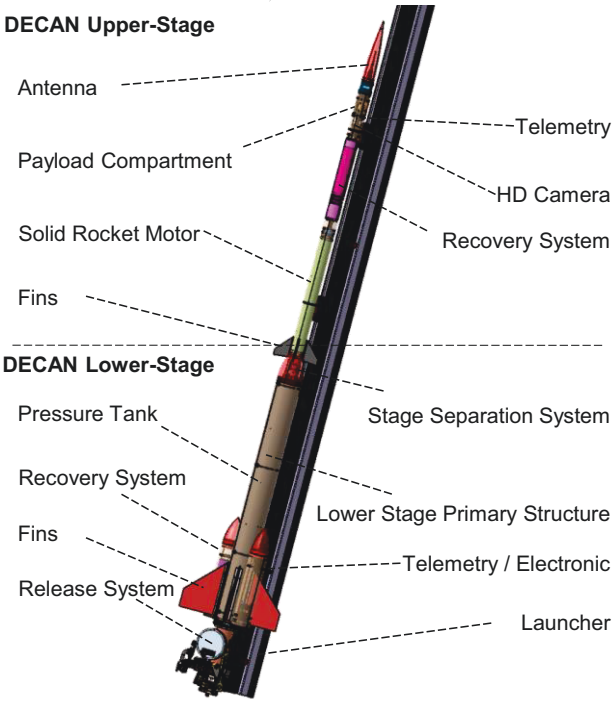

FIG 1. DECAN two-stage rocket and its main components

Both stages include recovery systems in order to ensure reusability. The lower stage recovery system is designed to carry both stages in the case of a malfunction of the stage separation system. FIG 2 shows the mission concept of DECAN two-stage sounding rocket. After release of the rocket, the exhaust (hot water vapor) accelerates the two-stage rocket. At the end of the accelerating phase, the lower stage is separated (2) and the upper stage solid rocket motor is ignited (3). The upper stage transports the

CanSat payload to a peak altitude of 7 km. At apogee, a payload, such as a CanSat, can be ejected (5). Both stages, as well as the payload, return with the support of a recovery system (4) (6) safely to the ground (7) (8).

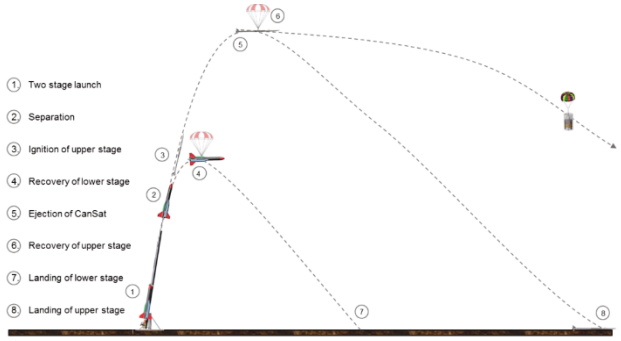

FIG 2. DECAN Mission Concept

3. LOWER STAGE – DECAN AQUARIUS

The propulsion system design of the first stage is based on experience gained from the TU Berlin AQUARIUS project which has been optimizing hot water propulsion systems for over two decades. During the heating-up phase, both pressure and temperature can be monitored for safety reasons. Several safety mechanisms were included in collaboration with the Technical Inspection Association (TÜV) to provide a safe working environment. Once the release system is triggered, the water jet is ejected and evaporates immediately within the nozzle due to lower external pressure. A calculated average thrust of 2.2 kN is provided for approximately 5 s, allowing the first stage to reach an apogee of approximately 1 km, which is high enough to allow frequent test flights in Germany. These performance values were supposed to be confirmed during the first test flight of the rocket in 2017.

3.1. Structure

The rocket structure is mounted to the vessel with frictionally-engaged retaining rings. Therefore, the vessel is not weakened, and the rocket can be assembled and disassembled easily. As seen in FIG 3, four equally spread fins enable a passive aerodynamic stabilization and are connected to the rings. Two compartments provide space for a suitable recovery system, electronic subsystems, and optional payloads. They are mounted to the rings as well. The recovery system is designed to recover the lower stage after a testflight, but it is also dimensioned in such a way as to allow recovery of both stages in case of a faulty stage separation. The load-bearing parachute rope is wired to the retaining rings and secured redundantly. An Altusmetrum telemetry board measures all relevant flight parameters such as acceleration and height during flight. It also transmits collected data to the ground via downlink. Once the apogee is reached, the board computer triggers the actuator to release the recovery parachute which is inflated by the help of a drogue parachute. A prestressed spring mechanism helps release the parachutes. An optional payload may be included in the electronics compartment. Following a design update, a second telemetry unit is used. It is completely designed and built by students and already successfully tested during the upper stage launch campaign at Kiruna. The electronics determine the rocket orientation, measure temperatures, the altitude, and the rocket's position. All data is transmitted to ground via 3G network or W-LAN.
The tail fins and compartment structures had to be moved in the direction of flight due to structural changes of the rocket in the last years, changing the aerodynamic behavior. Simulations have shown aerodynamic instability of the previous fin configuration. Therefore, the tail design process had to be reiterated.

3.2. Stability and Fin-design

The Barrowman-method was used to calculate the stability of the rocket.

$$c_{mn} = \frac{X_{CP} - X_{CG}}{d_R} \quad (1)$$

According to eq. 1 the stability margin (also called caliber) depends on the diameter of the rocket, which was not changed, and the locations of the center of pressure and center of gravity. Those parameters can be altered by adding mass to the front or the rear or by changing the geometry of the rocket, e.g. the size, shape, and location of the fins. One must consider that the location of center of gravity is moving during flight due to the use of propellant.

Using the semi-empirical Barrowman-method to calculate the center of pressure, a new fin design (FIG 3) could be made to ensure a stability margin at launch above 1.This rather unusual design was necessary to achieve the needed pressure point locations while complying with all constructional constraints. Those were caused by the limited space of the current launch tower configuration and the structural casing surrounding the nozzle, which is supposed to be easily accessible. Additionally, the fins were easy to manufacture. At the same time, the mass of the fins was reduced by using an aluminum composite material, which shifted the center of gravity further to the front and increased the stability.
The margin drops down to approximately 0.6 at the critical point. This is seen as unproblematic, since the margin is still positive, which means that the rocket should be stable during its flight. Additionally, the length/thickness- ratio is comparably low, leading to a smaller susceptibility of the trajectory by crosswinds.

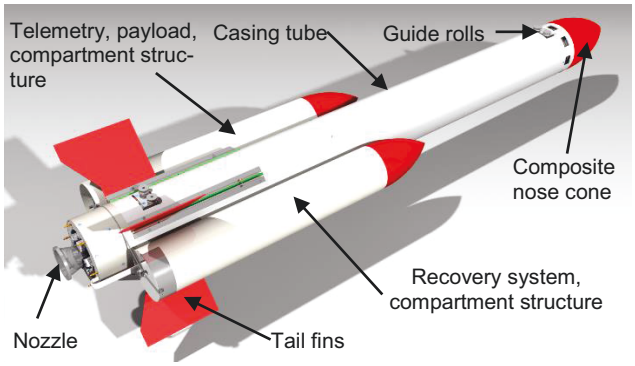

FIG 3. Current development status of TU-Berlin's DECAN lower stage (DECAN AQUARIUS).

3.3. Trajectory Simulation

The trajectory simulations were done with the open source program OpenRocket. If only the lower stage is launched, calculations of the trajectory predict a peak altitude of 533 m at a take-off weight of 94.8 kg and a launch angle of 80°. The maximum speed was calculated to be 89 m/s (0.26 Ma) at a maximum load factor of 1.9 g.

Parameter	Lower Stage
Rocket type	Hot water propulsion
Motor manufacturer	TU Berlin
Propellant	Water (29 liters)
Scientific payload	Telemetry system, positioning and locating system, cameras, heat and altitude measuring
Nominal diameter	ca. 0.2 m
Length	ca. 2.2 m
Liftoff-Mass	95 kg
Average thrust	Ca. 2.2 kN
Burning time	5 s
Maximum acceleration	1.9 g
Apogee altitude	533 m (single-staged)
Minimum stability margin	0.64(@0.26 Ma)

TAB 1. Technical data sheet of the lower stage

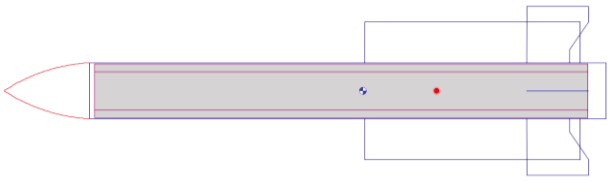

FIG 4. Sketch of DECAN'S lower stage in OpenRocket.

The motor's thrust curve had to be estimated roughly, since it is not a typical propulsion system and no test data was available. Therefore, it is an estimation based on experience with similar motors. The basic values of the motors, used for the simulations are:

- Total impulse: 1100 Ns
- Average thrust: 2210 N
- Burning time: 5 s
- Motor take-off mass: 78 kg
- Motor empty mass: 49 kg

The output of the trajectory simulation is shown in FIG 5. It can be seen, that the end of burning time goes along with a turning point of the altitude graph. The speed at the end of the burning time is at its maximum (90 m/s). After that, it decreases until it reaches the apogee. Due to the release

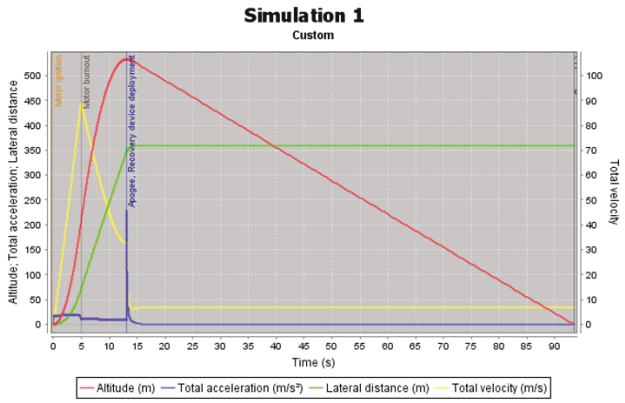

FIG 5. Total acceleration (blue), altitude (red), total velocity (yellow) and lateral distance (green) as a function of time

of the parachute in apogee and subsequent unfolding, the rocket's acceleration due to the gravitational force is stopped after a few seconds. The fall velocity is relatively constant from t=13 s (533 m) on until it reaches the ground. The landing speed is approximately 6.61 m/s. Given this data, the motor and most of the subsystems should be unharmed. The essential output parameters of this flight are given in TAB 2:

Parameter	Lower Stage
Max. altitude	533 m
Flight time	93.4 s
Max. speed	90 m/s
Max. acceleration	19 m/s^2
Max. Load factor (G-Load)	1.9
Time to apogee	13.1 s
Ground hit velocity	6.61 m/s
Lateral Distance	360 m

TAB 2. Output values of the trajectory simulation

3.4. Electronics Ground Segment

The lower stage is equipped with a FPGA (field programmable gate array) used as an on-board computer with an IMU (inertial measurement unit) to measure all relevant flight parameters such as acceleration, altitude, and angular velocity. It also transmits collected data to the ground via downlink. The lower stage also provides visual information by giving the opportunity to mount several cameras onto the tank. The downlink system is not capable of providing real time videos. Instead, each camera includes an up to 32 GB memory card to store video material which can be evaluated after the landing.
Before take-off, pressure and temperature must be monitored and logged for safety reasons. Thereby one pressure measurement unit and two temperature sensors are used to collect the data from the inside of the tank. All supporting electronic devices for the sensors such as power supplies and amplifiers are kept in an external container where all components are protected from water. The plug-and-play design of the box makes it easy for new students to understand and fast to learn, use, and assemble. Once assembled, the sensor data is captured by a data acquisition system to automatically write all collected measurement values to an data file where pressure and temperature are plotted in real time. Since there is one continuing file, all graphs from past tests and launches can be compared with the latest results.

3.5. Preparations

A critical design review (CDR) was held in late 2016 to finalize the CAD model after the stability calculations were successfully iterated.
The building process was accompanied by constant testing of the subsystems. Those tests dealt mostly with the sealing of the propulsion system and the recovery system.

Pressure tests were performed to prove flight readiness of the propulsion system. First, the fully filled tank was manually pressurized to 92.6 bar at room temperature to allow a safe leakage check. When this cold pressure test was completed successfully, a hot pressure test was per-

formed to ensure leak tightness under start conditions. Therefore, the rocket was additionally secured and heated until the desired pressure and temperature values were reached.
Additionally, the pyro actuator to open up the plug was extensively tested to ensure a safe release of the rocket at lift-off.
When the rocket was integrated sufficiently, the recovery system was tested in a wind tunnel test campaign.
This led to small necessary changes in the recovery system to ensure a safe opening of the parachutes. Finally, the recovery system was qualified to ensure an opening at the comparatively low estimated speeds at apogee.

A rehearsal was executed about one week before the launch to practice and validate all launch procedures, instructions, and checklists. This qualified the whole system as overall flight ready and allowed a more precise planning of the countdown procedures.

3.6. Flight Test (Launch Campaign)

The launch of the DECAN AQUARIUS took place on March 31st 2017 at Klietz, Saxony-Anhalt. Due to the prior preparations and testing, the launch procedures were executed without problems.
The launch tower was erected one day before the actual launch to allow the preparations of the rocket at the launch site without time pressure concerning the crew. The preparations of the rocket at the launch site are shown in FIG 6:

FIG 6. Preparations of the lower stage before the launch

When the sealing of the rocket was finished, a cold pressure test was successfully executed (more than 90 bar).
Afterwards, small changes were made to ensure flight readiness of the rocket. This included the start-up of the payload as well as the telemetry system. When all checks were completed, and therefore all systems “go”, the heating was started.
A pyro actuator was fired at 54.3 bar to unlock the rocket and the nozzle opened nominally. The exhausting water vapor accelerated the rocket.
Unfortunately, the chutes deployed, unfolded, and were ripped off during the lift off. Then the rocket continued its flight on a slightly less inclined trajectory. The engine stopped accelerating at about 3 s in flight.
After reaching the apogee, the rocket continued its ballistic trajectory to the ground. It showed some rolling (about 1 turn per sec.), but continued a stable flight.

3.7. Flight Data (Launch Campaign)

During the flight, the onboard telemetry system (Telemetrum board) recorded (100 samples/s) and transmitted (10 samples/s) measurement data in real time to the ground station.
The measured data for the whole flight can be seen in FIG 7. The resulting flight parameters are presented in TAB 3. The diagram presented in FIG 8 focusses on the acceleration phase of the rocket. It can be seen that the average acceleration during the launch phase was between 40-50 m/s². Therefore, the actual acceleration, and consequently the thrust, were twice as high as calculated.

An estimation of the resulting thrust is depicted in FIG 9. It was calculated using the assumption of a steady water mass flow of 8.9 kg/s. This follows out of the water mass of 29.5 kg and the burn time of 3.3 s. The higher thrust resulted also in a higher velocity than calculated.

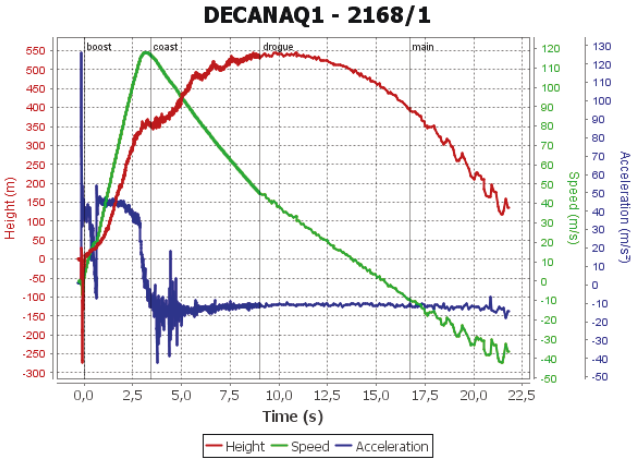

FIG 7. Measured flight data by the Telemetrum board; total acceleration (blue), altitude (red) and total velocity (green) as a function of time

Parameter	Lower Stage
Max. altitude	545 m
Flight time	21.6 s
Max. speed	118 m/s
Max. acceleration	126 m/s²
Max. Load factor (G-Load)	13.0 g
Time to apogee	10.6 s
Burn time	3.3 s
Lateral Distance	1100 m

TAB 3. Measured values during the flight

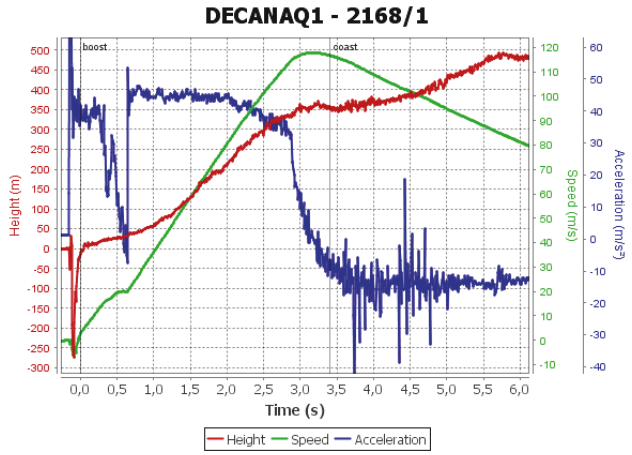

FIG 8. Measured flight data by the Telemetrum board during the launch phase

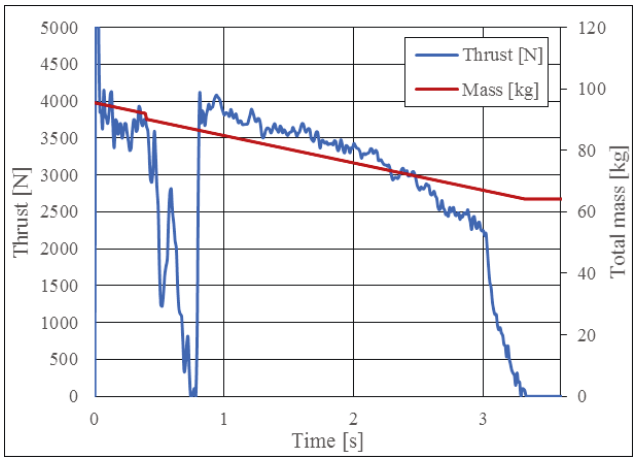

FIG 9. Estimated thrust development during the launch phase

3.8. Conclusions of Flight Test

The first full flight test of the completely new developed hot water rocket DECAN AQUARIUS was successful.
The created documents concerning the Assembly, Integration and Verification process (AIV), the launch preparation at the launch site and the countdown procedures were able to be validated.
Furthermore, most of the subsystems were able to be verified, except for the recovery system. First investigation showed that a structural part was damaged during lift-off.
High acceleration forces of up to 12 G's led to a structural failure of a mount that locks the opening mechanism. This opened the compartment and the chutes were ejected. The measured peak acceleration exceeded the calculated value, the average thrust was about 10-15% higher than nominal. The structure wasn't designed to withstand those stresses. Therefore, the locking mechanism of the recovery system needs to be reviewed and redesigned.
Another minor failure affects the telemetry system. No GPS signal was received. One of the reasons is probably the protecting aluminium case, which narrowed the field of view of the GPS antenna. Therefore, a redesign needs to be done. Since it was used to protect the Telemetrum board at impact following the test flight, this will not be necessary during future flights with a verified recovery system.
The GPS component of the FPGA payload was also not receiving any data at all. Since the payload was successfully tested before, a physical malfunction seemed to occur throughout the build-up process of the launch environment. The GPS antenna was attached to the inner face of the payload container. If the antenna has fallen off, it still would have had contact with the payload board but might have faced in the wrong direction. At this point the hot water tank would have had blocked the GPS signal and therefore, making the GPS receiver blind. A standardized mounting environment should prevent a reappearance of the error.
Despite the missing GPS-signal, the payload worked well. Therefore, acceleration data was recorded and also transmitted in real time during the flight.

The flight test also revealed optimization potential:
The fins could be optimized when a new locking mechanism and new launch tower are used. This allows a more aerodynamically tuned geometry of the fins, which would lead to less drag and therefore, a higher apogee.
Several nozzle geometries could be tested to verify the influence on the thrust development. Therefore, a hot water test stand could be built to test these hypotheses.
A safe and arm device needs to be integrated and tested to ensure a start campaign at Kiruna. While a mechanical one is already verified by the successful flight of the upper stage, an electrical one is in development.
Due to strict safety measures, no significant problems were recorded during the building process and launch campaign. Another test flight is planned, as soon as a new FM of the rocket is built. First of all, it is planned to expedite the development of the solid propellant upper stage.

4. UPPER STAGE - A 3D-PRINTED ROCKET

In order to assure an ongoing development of solid propellant rockets and frequent launch campaigns the project costs have to be optimized. Hence, the rocket design and campaign costs have been identified to bear the highest potential of cost reduction.

4.1. Rocket Design

The SHARK rockets were designed for traditional manufacturing processes. Therefore, hundreds of small parts have to be assembled to lager components. These small parts are manufactured with milling machines, which is time intensive. The selective laser sintering allows to 3D-print whole rocket segments as one part. Instead of manufacturing and assembling hundreds of parts, nine rocket segments are printed and easily assembled. The new rocket design is inspired by the SHARK rockets containing only slight changes regarding aerodynamics. It is designed to be a lightweight construction. The main differences to the original design are the increasing diameter of the main tube from 110 mm to 114 mm and a decreased lift-off mass of 4 kg in total. Hence, the primary structure mass is decreased by 50 %. The rocket will be able to carry three different motor sizes to ensure maximal flexibility. A demonstration model of the green segment, shown in FIG 10 was printed and can be seen in FIG 20.

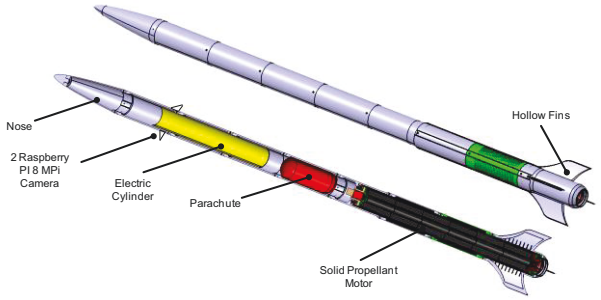

FIG 10. DECAN upper stage rocket and its main components

Parameter	Upper Stage
Rocket type	Solid propellant
Primary structure	3D-printed Alumide
Scientific payload	Telemetry system, video camera, CanSat
Nominal diameter	ca. 0.11 m
Length	ca. 2.7 m
Dry mass	10.8 kg
Primary structure mass	4.8 kg
Propellant Mass	7.7 kg
Maximum thrust	3 kN
Burning time	7 s
Maximum acceleration	17 g
Minimum stability margin	2

TAB 4. 3D-Printed rocket technical data sheet

4.2. Nosecone Design

Nosecones of commercial suppliers are made to fit the requirements of various customers with the least amount of different nose cone models. In many cases, this leads to the disadvantage of having to use a nose cone which is not exactly fitting the boundary conditions of the project. E.g. the last version of the shark rocket needed an adapter to make the commercial nose cone fit the wider radius of the body tube thus leading to increased weight and aerodynamic losses. 3D-Printing provides a cost-efficient and easy method to manufacture nose cones fitting the expected conditions. In this case, the nose cone shall provide minimum drag for the calculated Mach numbers and withstand the aerodynamic heating.
The aerodynamic drag of a rocket consists manly of three parts: base drag, skin friction, and wave drag, whereas the base drag in most configurations is not dependent on the nose cone. In low and mid subsonic flight, the total drag of a nose cone is mostly characterized by skin friction and thereby by the wetted area, the surface smoothness of that area, and discontinuities in the shape. In high subsonic flight, shockwaves start to appear, leading to increased wave drag, making it a major contributor to the total drag. The maximum wave drag is typically reached around Mach 1 and decreases afterwards. Wave drag is mostly depending on the shape of the nose cone, the fineness ratio and the free stream Mach number.
To reduce skin friction in subsonic flight, it might be necessary to reduce the wetted area which may collide with interests of reducing the wave drag (depends on shape). Since the wetted area of the nose cone is small compared to the body tube we are going to neglect low and mid subsonic flight and only focus on transonic and supersonic Mach regions. Other methods of reducing skin friction (e.g. surface smoothness) are not affecting wave drag. As a result, 3D-Printing allows to adjust the aerodynamic drag through two parameters: shape and fineness ratio (if the flown Mach numbers are fixed).

4.2.1. Choosing the nose cone shape

A collection of commonly used nose cone shapes including a qualitative comparison is provided by [1]. It is important to note that each shape has its advantages and disadvantages compared to the other shapes in certain Mach regions, so there is no perfect shape for all conditions. FIG 11 shows the expected Mach number distribution according to an OpenRocket simulation.

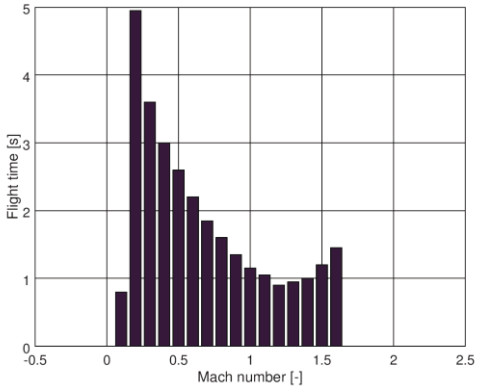

FIG 11. Mach number distribution for the expected trajectory

According to [1] there are two shapes qualifying for the Mach distribution shown in FIG 11. It's the Von Karman Ogive and the x1/2 power series. The Von Karman Ogive is a theoretically derived shape yielding the minimum drag in supersonic flight. Its best applied in Mach numbers ranging from 1.5 to 3.0. In the transonic region, which is difficult to calculate and a major part of the given Mach number range, the power series is slightly outperforming the Von Karman Ogive. Reference [2] provides experimental data on the drag coefficient over Mach number for both shapes. This makes it possible to run an OpenRocket simulation to quantify and compare the performance of both shapes in the given Mach number range. OpenRocket uses the drag coefficient curves from [2]. Flight height over time results are shown in FIG 12.
It shows that there is only minor difference between the two shapes. The apogee differs by 18 m in favor of the power series shape.

Besides the shape, the performance of the nose cone is also influenced by the fineness ratio. It is defined as the ratio between the total length of the nose cone and the base diameter (L/D). Since the base diameter of the body tube is fixed it is only possible to adjust the length of the nose. Reference [3] states that the drag coefficient of nose cones is decreasing with increasing fineness ratio. Furthermore, a fineness ratio of 3 is recommended for good balance between decrease in drag and additional mass. This fits very well with the available space in the 3D-printing chamber of 35 cm. A base diameter of 11.4 cm

and a fineness ratio of 3 yields a total length of 34.2 cm.

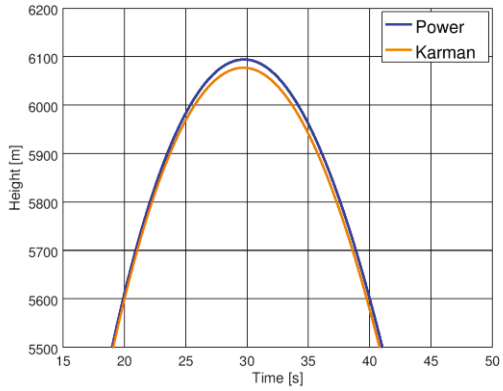

FIG 12. Simulated trajectory near apogee for Von Karman shape and power series

4.2.2. Reinforcing the tip due to aerodynamic heating

Aerodynamic heating accrues basically due to two phenomena: compression of air in the stagnation point and viscous deceleration of the air in the boundary layer (skin friction). These phenomena rely on the same physical principal of kinetic energy being converted to internal energy. Areas near the stagnation point will derive most of their heating from the compression of air while areas far away from the stagnation point will derive it mostly from viscous deceleration [4]. Since the velocity in the stagnation point is zero, all kinetic energy is converted to internal energy and is therefore added to the local static enthalpy. The temperature in the stagnation point for an adiabatic reduction of velocity is given by eq. 1 and is called total air temperature or stagnation temperature.

$$T_t = \left(1 + \frac{\kappa - 1}{2} Ma^2\right) T_s \qquad (2)$$

Tt = total air temperature
K = heat capacity ratio
Ma = Mach number
Ts = static temperature

According to [4], areas near the stagnation point will not have much variation in temperature normal to the surface. This is because the air is compressed in front of the rocket rather than being brought to rest due to the no-slip condition in boundary layers. This means that there is a large supply of heat energy near the stagnation point, so that any conduction of heat away from the skin will be quickly replenished. Boundary layers far away from the stagnation point on the other hand are very thin compared to the size of the rocket and have a significant temperature gradient. Only the air exactly at the skin is brought to complete rest. From there the temperature is falling with growing distance to the skin until it reaches free stream conditions at the outer edge of the boundary layer. This indicates that there is little heat generation capacity and as a result, the amount of heat conducted away from the boundary layer will strongly affect the temperature of the surface of the rocket. This is covered by adding an empirical obtained recovery factor e to eq. 1 which is shown in eq. 2.

$$T_t = \left(1 + \frac{\kappa - 1}{2} e Ma^2\right) T_s \qquad (3)$$

For the stagnation point, e = 1. Besides that, the recovery factor is always smaller than 1. This means that the highest air temperature is reached near the stagnation point and therefore is the highest skin temperature also reached at the stagnation point. The total air temperature over flight time for the given OpenRocket simulation is given in FIG 13.

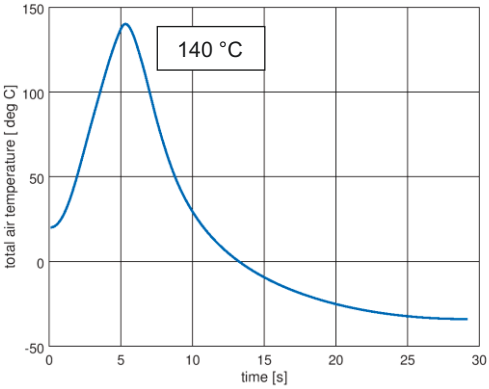

FIG 13. Total air temperature distribution for the expected trajectory

The maximum total air temperature reached in the stagnation point is 140 °C. Measurements from the past launch campaigns showed an approximate error of 5 % to the OprenRocket simulation. To fulfill the safety requirements, stating that a safety factor of 2 is required, +10% were added to the velocities obtained by the simulation.
TAB 5 shows the available thermic material specifications for the used alumide [5].

Parameter	Value
Melting point (20°C / min)	176 °C
Vicat softening point	169 °C

TAB 5. Thermic material specifications for alumide [5]

The maximum reached total air temperature is far lower than the melting point and the Vicat softening point. This means that the rocket nose cone will never reach these critical temperatures for the given velocities. A reinforcement of the nose cone tip due to aerodynamic heating is therefore not necessary. Since the total air temperature is only reached in the pressure point, the results also show that alumide is generally capable of withstanding the aerodynamic heating along the complete rocket.

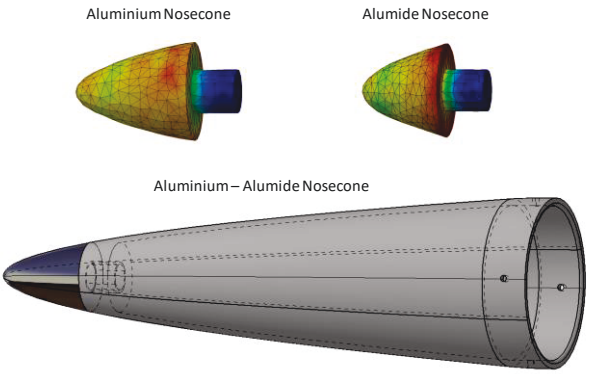

FIG 14. FEM Simulation of different nosecone materials

4.3. Flight Performance

A flight simulation was done in OpenRocket to compare the projected altitude of the former SHARK and the improved 3D-printed version and is presented in FIG 15.

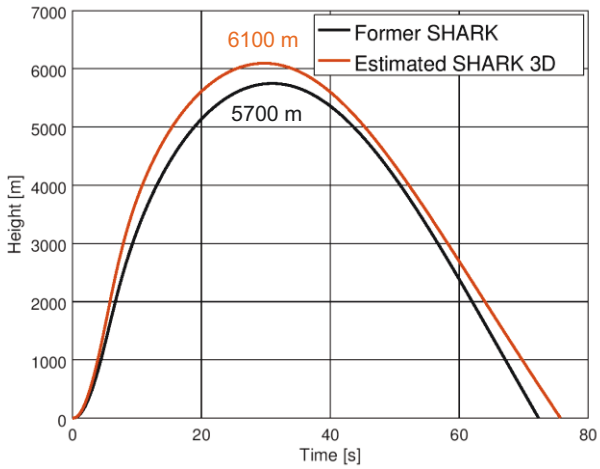

FIG 15. Comparison of simulation results for the flight of the conventional and 3D-printed SHARK

4.4. Structural Calculation

The knowledge gained from material tests and aerodynamic calculations can be used to perform first structure analyses. The critical property is the safety against buckling. Luckily, the 3D-printing offers easy possibilities to stiffen the rocket using a honeycomb sandwich structure. The design will be finalized in the near future.

The selective laser sintering technology is still relatively new. There is still a lack of knowledge regarding standards and databases. Hence, the quality of manufactured parts depends on the used printer and settings. Therefore, material tests have been performed at Fraunhofer Applications Centre for Large Structures in Production Technology AGP according to DIN EN ISO 527-2. The samples were kindly sponsored by Fabb-It. During motor tests, the heat build-up outside of the motor case stayed under 20 K and of the nozzle under 70 K. Hence, synthetic materials can be used for the primary rocket structure. To ensure a low-cost production, only adequate materials under 1.5 €/cm³ production cost were picked. Four print directions where investigated. Tree directions have been printed in the xy-plane to investigate the homogeneity of the material. The fourth direction is upright to investigate the merge of the layers. The empirical variance of the samples has been under 5 %, demonstrating high quality and reproducibility of the samples.[6]

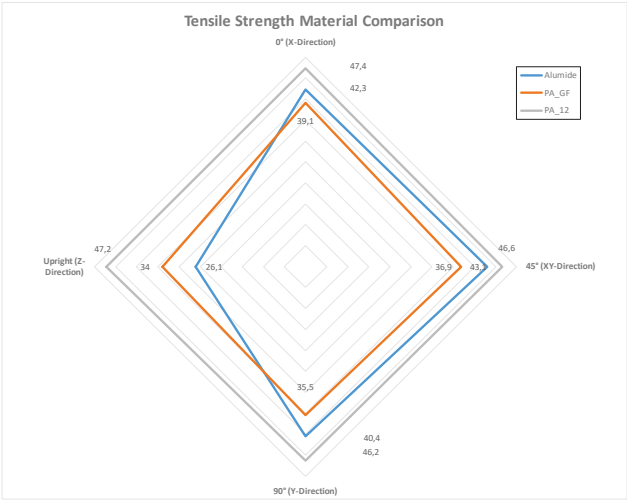

FIG 16. Tensile Strength material comparison depending on print direction [6]

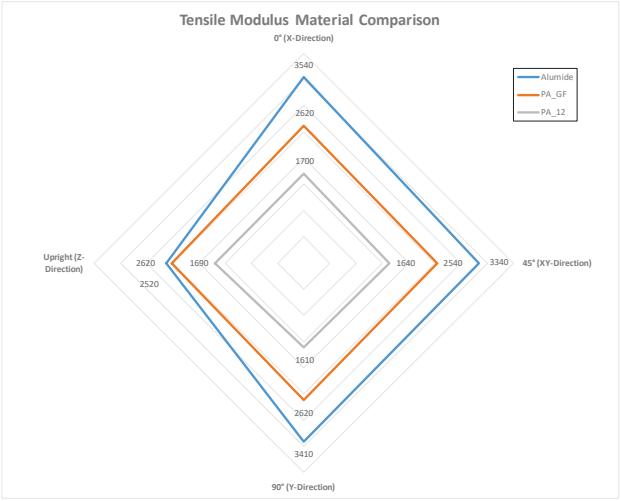

FIG 17. Tensile Modulus material comparison depending on print direction [6]

A honeycomb sandwich structure, shown in FIG 18, allows light weight construction, while a high stiffness is maintained. Due to the used selective laser sintering technology, no cavity can be manufactured. Hence, Hexagon openings are used to release the superfluous powder from inside of the honeycombs.

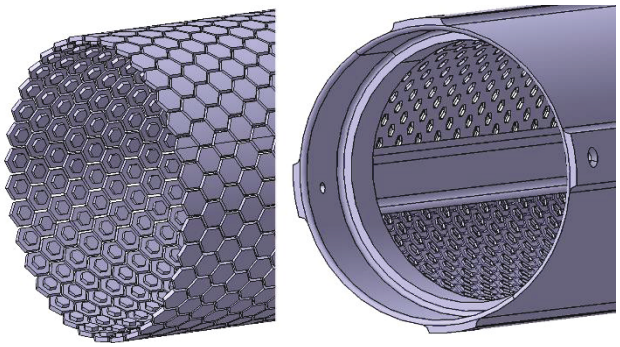

FIG 18. Left: negative CAD model of the honeycomb structure; Right: CAD of one segment

FIG 19 shows the von-Mises tension of the primary rocket structure using a honeycomb sandwich structure. A safety factor up to yield point of 2.5 and a safety factor against buckling of 2.8 are assured.

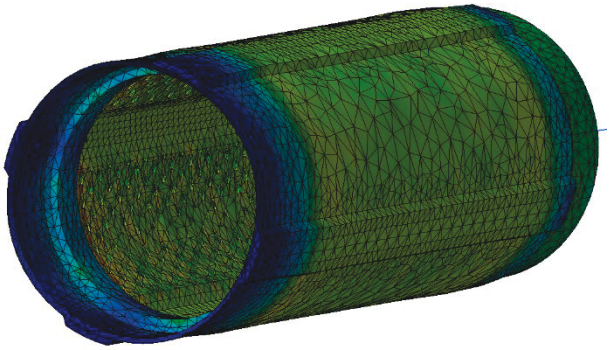

FIG 19. FEM Simulation of one segment

Based on these considerations, and taking the low production cost into account, 3D printing offers a great potential for future rocket projects.
FIG 20 shows pictures of a 3D-printed demonstration model, sponsored by Fabb-It. The model is highly accurate with a deviation of under 0.15 %. Structural tests will be performed in the near future to validate the simulation methods.

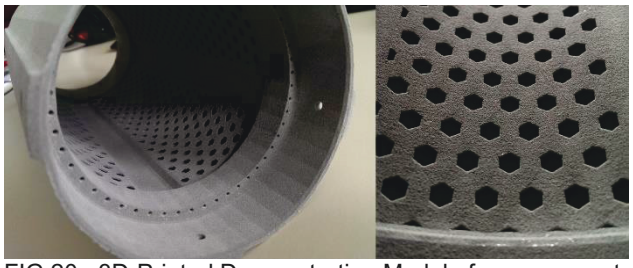

FIG 20. 3D-Printed Demonstration Model of one segment

4.5. Electrical Safe and Arm Device

One of the novelties during the last months of development was the design of the new electrical Safe and Arm Device (S&A). The S&A is intended to be flown with both the upper and the lower stages. The first task of the S&A is the interruption of the flow of current between the electronics and the power supplies during the launch preparations. The second task is to short circuit the Electrical Explosive Devices (EED's). If both tasks are fulfilled, the rocket is in SAFE mode. That means no subsystem of the rocket can cause any injury to personnel or damage to property. It ensures the safety during the assembly phase at the launch pad. The unlocking or arming of the rocket only takes place when the rocket assembly is completed and all team members and other people have left the danger zones. Switching to the armed mode happens in two single steps. First of all, the power supply is connected to the electronics. If this is successful (telemetry reports a valid GPS position), the second step will be initiated. This step connects the EED's with the electronics. The splitting is necessary to avoid an uncontrolled ignition of the rocket motor by the on-board electronics in the event of a failure within the electronics. After the activation of the S&A, it is not allowed to enter the danger zones (around the launch pad) because the rocket is in armed mode and thus ready for launch. In case of a necessary access to the danger zone (e.g. if the launch was not successful), the S&A has to deactivate the electronics and short the EED's. At this point, it is safe to approach the rocket to look for possible issues. This will allow readying of the rocket launch again and the procedure will be started anew. The S&A is operated from the user's lab (ESRANGE), outside the danger zones. [7] [8]

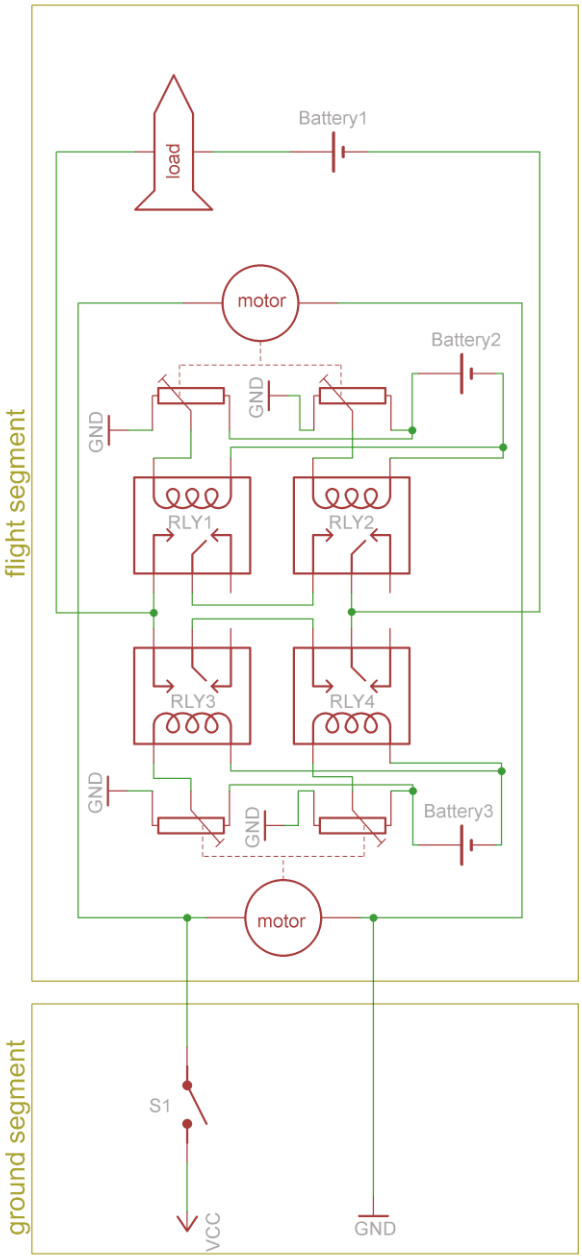

FIG 21. Schematic Circuit Diagram

The S&A consists of two main segments. These are the flight segment and the ground segment. The flight segment (FS) is incorporated in the DECAN rocket, both in the first and in the second stage. The FS consists of two individual S&A devices, one of which controls the electronics, telemetry system and also the payload, e.g. CanSat compartment. The second S&A device is in charge of arming / disarming the pyrotechnics system (EED). These two modules can be activated individually by their respective counterpart (the S&A Switch), which is located on the

ground segment. FIG 21 shows a schematic circuit diagram.

Modus Operandi:

1. Switch S1 is closed.
2. The motors potentiometers are powered and therefore the resistant is constantly decreased, leading to a rise of the voltage inside the relays.
3. As soon as the voltage is high enough, the relays will close. The load circuit inside the rocket (Payload, SED etc.) is now closed.
4. The rocket is armed and ready for launch. During launch, the connectors between flight- and ground segment are disconnected.
5. The rocket can be set to safe mode, in case of a launch aboard. Therefore, the polarity of the ground segment has to be reversed.

The electrical Safe & Arm Device is designed to be single failure tolerant.

Parameter	Mechanical S&A	Electrical S&A
Single failure tolerant	No	Yes
Mass of flight segment	1.5 kg	1 kg
Mass of ground segment	30 kg	0.2 kg
Cost of flight segment	400 €	130 €
Cost of ground segment	2500 €	20 €

TAB 6. Comparison of the old mechanical and the new electrical Safe and Arm Device

4.6. Raspberry Pi Camera System

The successfully launched SHARK I&II rockets possessed a GoPro Camera, that allowed to capture the flight through a side window. Due to its size, it could only be positioned in a way that the horizon could be filmed, which did not allow the team to analyze footage of the early deployment of the parachutes
The new system consists of two far smaller 8 MPi Raspberry Pi Cameras, allowing it to be positioned downwards. Hence, the rocket launch and all release systems can be seen in a better angle. Furthermore, a constant downlink will provide live footage of the flight.

5. CONCLUSIONS

This work describes the current development of the DECAN rocket at the Technische Universität Berlin. The different components of the rocket were explained in detail. The AIV-process and launch campaign of the hot-water lower stage were elaborated. Additionally, the flight data from the first test flight were presented. Features such as the newly developed 3D-printed rocket structure were shown. This also includes the presentation of the first 3D-printed segment as a demonstration model.

6. ACKNOWLEDGEMENTS

The authors would like to thank Prof. Brieß and Dr. Harry Adirim as well as the DLR MORABA team for their support. This work was funded by the DLR's STERN project. We like to thank Aerospace Institute, Fabb-It and Fraunhofer. Our student project would not be possible without their sponsorship efforts.

Bibliography

[1] S. S. Chin, Missile Configuration Design, USA: McGraw-Hill Book Company, Inc., 1961.

[2] W. E. Stoney, „Transonic Drag Measurements Of Eight Body-Nose Shapes," NACA, Washington, 1954.

[3] J. William E. Stoney, „Collection Of Zero-Lift Drag Data on Bodies of Revolution," NACA, Washington, 1958.

[4] G. F. R. Duarte, M. G. d. Silva und B. d. M. Castro, „Aerodynamic Heating Of Missile/Rocket - Conceptual Design Phase," 20th International Congress of Mechanical Engineering, Gramado, Brazil, 2009.

[5] EOS GmbH - Electro Optical Systems, „Datenblatt Alumide," [Online]. Available: http://fkm-lasersintering.de/images/pdfdaten/Alumide.pdf. [Zugriff am 15 08 2017].

[6] T. Nitschke, H. Adirim, A. Balke, J. Léglise, E. Melan, M. Riekeles, M. Schmid und P. Wüstenberg, „LAUNCH CAMPAIGN OF THE DECAN UPPER & LOWER STAGE AND DEVELOPMENT OF A 3D-PRINTED EXPERIMENTAL ROCKET AT TU BERLIN," Deutscher Luft- und Raumfahrtkongress, Braunschweig, 2016.

[7] T. Nitschke, J. Kolbeck, R. Wolf, R. A. Court, P. Wüstenberg, E. Melan und M. Schmid, „THE DECAN PROJECT AT TU BERLIN," Deutscher Luft- und Raumfahrtkongress, Rostock, 2015.

[8] O. Widell, „Esrange Safety Manual," Swedish Space Corporation, Kiruna, 2014.

Gefördert durch:

Bundesministerium
für Wirtschaft
und Technologie

Fraunhofer

aufgrund eines Beschlusses
des Deutschen Bundestages

FKZ: 50 RL 1251

AI:
Aerospace Institute

DLR Deutsches Zentrum
für Luft- und Raumfahrt
German Aerospace Center

STUDENTISCHE EXPERIMENTAL-RAKETEN • DEUTSCHES ZENTRUM FÜR LUFT- UND RAUMFAHRT (DLR)
STERN

SSC

Fabb-It

Astos
Solutions